Magnon Blocking Effect in an Antiferromagnet-Spaced Magnon Junction

Z.R. Yan,[1,2,†] C.H. Wan,[1,†] and X.F. Han[1,2,3,*]

[1] *Beijing National Laboratory for Condensed Matter Physics, Institute of Physics, Chinese Academy of Sciences, Beijing 100190, China*

[2] *Center of Materials Science and Optoelectronics Engineering, University of Chinese Academy of Sciences, Beijing 100049, China*

[3] *Songshan Lake Materials Laboratory, Dongguan, Guangdong 523808, China*

(Received 23 July 2020; revised 7 September 2020; accepted 29 September 2020; published 28 October 2020)

We study magnon transmission in the sandwich structure of ferromagnetic insulators (FMIs), antiferromagnetic insulators (AFMI), and ferromagnetic insulators (FMI) by atomistic spin-model simulations. Magnon junction effects (MJEs), which have been reported in magnon junction (MJ) experiments, can be reproduced in this work, demonstrating the importance of spin-dependent magnon blocking effects (MBEs) in a MJ structure. Moreover, AFMI spacers with various structures are investigated. We show that the MJE is sensitive to the characteristics of the AFMI spacer such as orientation of Néel vector, types of AFMI spin configuration, and intrinsic exchange interaction. It is found that these phenomena are rooted in the magnon selection rules between two FMIs of different magnonic polarization. Based on the mechanism studied above, we further propose an in-plane MJE and give a feasible experimental prediction using nonlocal magnon-mediated current-drag measurement. Our work provides insight into magnon transmission in MJ and serves as a promising tool for future magnon circuits.

DOI: 10.1103/PhysRevApplied.14.044053

I. INTRODUCTION

Spin wave (or magnon when quantized)—the collective excitation in a magnetically ordered system—is a promising candidate for information carriers [1–3]. It can deliver angular moment over a long distance of several tens of micrometer to even millimeters [4–6]. Owing to the absence of Joule dissipation, it can principally transfer angular moment with high-energy efficiency [3]. On the other hand, various magnon injection and detection techniques have been demonstrated [7–15]. For instance, microantenna can generate and detect coherent magnon with fixed frequency and phase based on electromagnetic effects [7,8], while heavy metals are widely used to inject thermal incoherent magnons by spin Hall effect and detect them by inverse spin Hall effect [9–15]. Besides, propagating magnons can be controlled via versatile manners such as magnetic field [13,14,16,17], current-induced spin transfer or spin-orbit torques [18–22], and even voltage-controlled magnetic anisotropy [23]. The wide physical toolbox seems already to offer us an opportunity to design magnon-based elementary devices on which future magnon electronics will be built on.

For example, a magnon valve effect (MVE) and magnon junction effect (MJE) were recently discovered [13,14] in the ferromagnetic-insulator–spacer–ferromagnetic-insulator (FMI-*S*-FMI) sandwiches in which the spacer *S* can be nonmagnetic metals (NMs) [13], antiferromagnet insulators (AFMIs) [14,24–26], or even domain walls [17,27]. In the MVE and MJE, output magnon current depends on parallel or antiparallel spin configuration of the FMI layers. Some other elementary devices such as magnon transistors [13,14,28–30] and magnon spin valves [31], which can regulate output signal by spin configuration or control magnon transport by current have also been creatively proposed and experimentally realized. Here we focus only, from a theory viewpoint, on magnon transport properties of the sandwich FMI-AFMI-FMI structure, which shares similarity with its spintronic cousin giant magnetoresist (GMR) or tunneling-magnetoresistance (TMR) based spin valves and magnetic tunnel junctions [32–38]. We uncover the physical mechanism via which the magnon valve (MV), especially magnon junction (MJ) structure, can regulate magnon transport by parallel (P) and antiparallel (AP) states.

In order to keep the system simple and physics clean, we restrict ourselves to the following three aspects. (1) A FMI-AFMI-FMI MJ structure such as the YIG/NiO/YIG system [14,26] was treated here. In this all-insulating system, angular momentum can only be delivered by

*xfhan@iphy.ac.cn

†Z.R.Y. and C.H.W. contributed equally to this work.

magnons without contamination from ordinary electron and spin current. (2) While the two YIG layers function both as magnon sources via spin Seebeck effect in the YIG/NiO/YIG experiment as in Refs. [13,14] and Ref. [26], we can conveniently set only one YIG layer as a single magnon source in theory. This unisource case has rarely been tried in theory before [25]. This treatment enables us to focus magnon transmission controlled by spin configurations only. We did not have to subtract an additional magnon current from the total magnon current due to the second magnon source. (3) We deal with incoherent thermal magnons instead of coherent magnons. In all of the MJ and magnon transistor experiments [13–15,19,21,39], only thermal magnons were utilized. While coherent magnon regulation by a magnon spin valves was investigated in Ref. [31], the counterpart effect for incoherent thermal magnons has rarely been reported yet [25].

Motivated by the previous experiments and theoretical deficiency [13–15,24–26,31], we systematically study the physics in MJ, fulfilling the above three conditions: thermal magnon transmission controlled by all-insulating magnetic structures with a unimagnon source. In our model we find that the MJE is due to magnetization-restricted magnon polarization [or magnon blocking effect (MBE) for short]. Besides depending on FMI magnetization, magnon transmission in a MJ can also be influenced by different spin lattices of the AFMI spacer. Moreover, we propose an in-plane MJ device based on nonlocal magnon-mediated current-drag measurement. Our work uncovers the physical details inside MJ and provides a guideline to choose suitable spacers for robust and large MJE.

II. MODEL AND METHOD

We focus on a MJ model with a unimagnon source, as shown in Fig. 1(a). It is noteworthy that compared to a temperature gradient across the whole MJ, a temperature step dropped only on the top FMI layer is applied to generate magnon current [40,41]. The temperature step as a single magnon source is helpful to understand the magnon transport properties of a MJ because the regions outside the temperature step function only as magnon conductive channels instead of magnon sources [40,41]. A free layer is introduced to construct P and AP states. The collective excitations of the upward (downward) magnetic order in simple ferromagnets precess only right- (left-) handed circularly.

In particular, an AFMI spacer with three types of spin lattices, as marked by A, B, and C, are studied. They are defined by their own spin configurations. Antiferromagnet with the type-A spin configuration has AFM orders along the z axis and FM orders in the x-y plane. Type B shows AFM orders in the y-z plane and FM orders along the x axis. Type C is a typical Néel order, which shows the

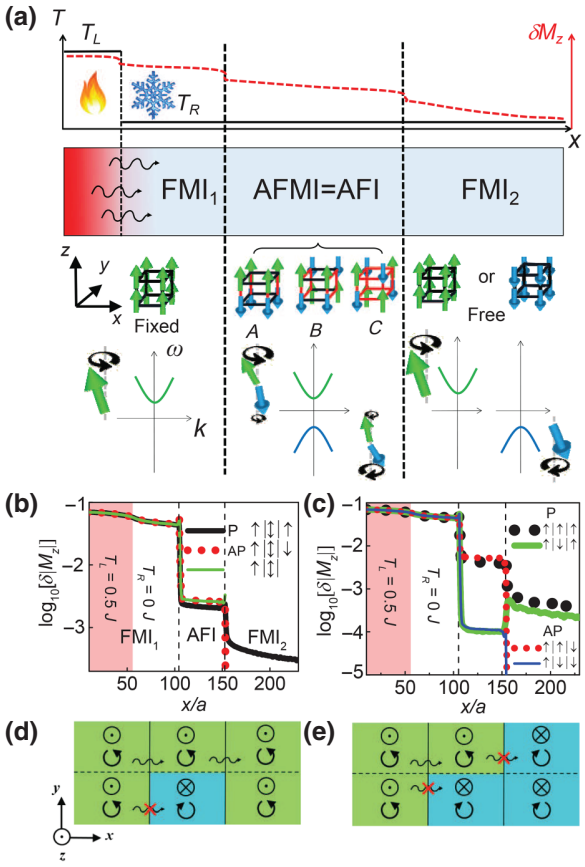

FIG. 1. Magnon junction structure and space dependence of magnon potential. (a) Illustration of the introduced temperature step (black solid line) and magnon potential (red dash line). The green vectors are for spin up (⊙) accommodating right-handed polarization (↻) of spin waves and blue for spin down (⊗) accommodating left-handed polarization (↺) of spin waves. FMI_1 is a fixed layer and FMI_2 is a free layer. Three types of AFMI marked as A, B, and C are considered, respectively. The red and black bars show antiferromagnetic coupling and ferromagnetic coupling between spins. AFMI can excite both right-handed and left-handed spin waves. (b) Magnon potential ($\delta|M_z|$) as a function of layer (x) of P state (black solid line), AP state (red short dot), and FMI_1-AFMI system (green line) at $J_c = 0.3$ J, $T_L = 0.5$ J, and $T_R = 0$. (c) Separated channel dependent ($\delta|M_z|$) from (b): ↑ | ↑ | ↑ (black dot), ↑ | ↓ | ↑ (green line), ↑ | ↑ | ↓ (red dot), and ↑ | ↓ | ↓ (blue line). (d),(e) Schematics of spin-dependent magnon blocking of P and AP state, respectively.

AFM order along the x, y, and z axes. Their configurations are constructed due to the special nearest exchange interaction. The types of the exchange interaction are marked by different color bar. Take type A as an example, it is a stable AFM order due to AFM coupling (red bar) along the z axis and FM coupling (black bar) within the x-y plane. Other AFM orders can be obtained by a similar setting of exchange coupling. The influences of other types of collinear AFM configurations are similar, so we discuss

only the three types of spacer. Qualitatively, the magnon mode of the three types of AFM configurations are similar, as shown in the sketch map of the ω-k function, suggesting that they can excite both right-handed and left-handed spin waves. Other types of AFMI spacer with nonlinear spin lattices would lead to extra and complex effects and need further investigation in future works.

We adopt the atomistic Hamiltonian based on a simple cubic Heisenberg model with localized normalized magnetic moment $\mathbf{S} = \boldsymbol{\mu}_s/\mu_s$, leading to

$$H = -J_{\mathrm{FMI}} \sum_{\langle i,j \rangle} \mathbf{S}_i \cdot \mathbf{S}_j - J_{\mathrm{AFMI}} \sum_{\langle m,n \rangle} \mathbf{S}_m \cdot \mathbf{S}_n - J_{\mathrm{FMI\text{-}AFMI}} \sum_{\langle i,m \rangle} \mathbf{S}_i \cdot \mathbf{S}_m - d_z \left[\sum_i (S_i^z)^2 + \sum_m (S_m^z)^2 \right]. \quad (1)$$

Here $J_{\mathrm{FMI}} = J = 1$ ($|J_{\mathrm{AFMI}}| = 1$) is the normalized nearest-neighboring Heisenberg interaction in (anti)ferromagnetic layers and $J_{\mathrm{FMI\text{-}AFMI}}$ is the interfacial coupling energy between the FMI and the AFMI layers. It is noteworthy that tuning J_{FMI} or J_{AFMI} within a reasonable range does not influence the main results, demonstrating the universality of our model. The fourth term on the right-hand side is the uniaxial anisotropy energy with $d_z = 0.01$ J. Dynamics of the considered spin model are simulated based on solving the following stochastic Landau-Lifshitz-Gilbert equation (2) [42]:

$$\frac{\partial \mathbf{S}_i}{\partial t} = \frac{\gamma}{\mu_s(1+\alpha^2)} \mathbf{S}_i \times [\mathbf{B}_i - \alpha(\mathbf{S}_i \times \mathbf{B}_i)], \quad (2)$$

where γ is the gyromagnetic ratio layer and α is the phenomenological damping constant. The effective field $\mathbf{B}_i$ is given by $\mathbf{B}_i = -\partial H/\partial \mathbf{S}_i + \xi_i(t)$ where $\xi_i(t)$ is the so-called white-noise field induced by thermal fluctuation [43]. The simulations are based on the numerical integration of the stochastic Landau-Lifshitz-Gilbert equation using Heun's method with a time step $\Delta t = 2 \times 10^{-4}\ |\mu_s/\gamma J|$. Simulation time in this work is nondimensionalized by unit of $|\mu_s/\gamma J|$ and its real value is decided by the parameters of materials. For example, for a typical value $J = 4.3 \times 10^{-21}$ J and $\mu_s = 2.65 \times 10^{-22}$ A/m^2 of YIG, the time step Δt is 0.07 fs. Such an approach and accuracy of simulation time step is well accepted and has been used extensively as a standard scenario for both ferromagnetic and antiferromagnetic systems [42]. To investigate magnon diffusion and transmission through the whole MJ, small damping constant $\alpha = 0.001$ as reported in the experiments [5] is used [40,41]. We consider an across section of 12×12 spins with periodic boundary condition, large enough to minimize finite-size effects [40,41]. The thickness of different layers are set as $L_{\mathrm{FMI1}} = 108$, $L_{\mathrm{AFMI}} = 48$, and $L_{\mathrm{FMI2}} = 108$ in the x direction. Other thickness combinations lead to no fundamental differences. The above-mentioned temperature step in the middle of FMI_1 ($x = 54$), as a single magnon source, divides the system into two parts: the hot region as a magnon source at the temperature T_L and the cold region as a magnon channel at T_R. Reasonably, an incoherent magnon source induced by spin Hall effect as adopted in the magnon-mediated current-drag experiments [9–12,15] is equivalent to the one used in this model. Space-dependent magnon potential $\delta|M_z(x)|$ defined as the difference between the absolute local magnetization $|M_z(x)|$ and its equilibrium value $M_z[T_R]$ relating to T_R is used to evaluate magnon accumulation and transmission as shown in Eq. (3) [40,41]

$$\delta|M_z(x)| = |M_z(x)| - |M_z[T_R]|, \quad (3)$$

where $|M_z(x)| = \langle \sum_{i \in x} |S_z^i| \rangle$ and $\langle \ldots \rangle$ denotes the thermal average. Total simulation time is 14 000 $|\mu_s/\gamma J|$, thereinto 4000 $|\mu_s/\gamma J|$ are used to reach the equilibrium state and another 10 000 $|\mu_s/\gamma J|$ steps are retained for statistical averaging. For the material YIG, the total time is about 4.9 ns. To evaluate the magnon accumulation in FMI_2 induced by the transmitted magnon from FMI_1 to FMI_2, we calculate average magnon potential in the bulk region of FMI_2 layer $\delta|M_z|_{\mathrm{FMI2}} = \sum_{x \in \mathrm{FMI2}} \delta|M_z(x)|$ where $L_{\mathrm{FMI1}} + L_{\mathrm{AFMI}} + 10 < x < L_{\mathrm{FMI1}} + L_{\mathrm{AFMI}} + L_{\mathrm{FMI2}} - 10$. The other definition of $\delta|M_z|_{\mathrm{FMI2}}$ does not significantly influence the conclusion of this paper, though there exists minor quantitative differences. Generally, the switching on:off ratio of transmitted magnon from FMI_1 to FMI_2 between P and AP state in MJ, called magnon blocking ratio (MBR), can be defined as

$$\mathrm{MBR} = (\delta|M_z|_{\mathrm{FMI2},P} - \delta|M_z|_{\mathrm{FMI2,AP}})/\delta|M_z|_{\mathrm{FMI2},P}, \quad (4)$$

where $\delta|M_z|_{\mathrm{FMI2},P}$ ($\delta|M_z|_{\mathrm{FMI2,AP}}$) is calculated $\delta|M_z|_{\mathrm{FMI2}}$ in P (AP) state.

III. RESULTS AND DISCUSSIONS

Type-A AFMI spacer is considered first and space-dependent magnon potential $\delta|M_z(x)|$ is shown in Fig. 1(b). Evidently, sharp $\delta|M_z|$ steps between the FMI and AFMI interfaces are observed, indicating strong interfacial magnon-scattering effects due to small interfacial coupling strength $J_c = 0.3$ J. In fact, J_c could strongly influence magnon transmission through the interfaces, which is investigated in detail later. Furthermore, a huge difference of $\delta|M_z|_{\mathrm{FMI2}}$ in FMI_2 between P ($\delta|M_z|_{\mathrm{FMI2},P} \approx 4 \times 10^{-4}$) and AP ($\delta|M_z|_{\mathrm{FMI2,AP}} < 1.0 \times 10^{-8}$) state is obtained and MBR ≈100%, showing the MJE [13,14].

For comparison, we also simulate an FMI_1-AFMI-vacuum system without the FMI_2 free layer in the same condition. Coincidently, $\delta|M_z(x)|$ distribution in the FMI_1-AFMI-vacuum system is nearly the same as the

AP state of the FMI_1-AFMI|FMI_2 MJ, indicating that the AFMI-FMI_2 interface in the AP state is as effective as an AFMI-vacuum interface in blocking magnon current.

Then we separate the P (AP) state of a MJ into two channels ↑ | ↑ | ↑ and ↑ | ↓ | ↑ (↑ | ↑ | ↓ and ↑ | ↓ | ↓) for type-A spacer [Fig. 1(c)]. Remarkably, the ↑ | ↑ | ↑ channel in the P state shows relatively high transmission, which accounts for the high magnon conductance in the P state. In contrast, both ↑ | ↑ | ↓ and ↑ | ↓ | ↓ channels in the AP state have a ↑ | ↓ interface, which leads to a MBE and low magnon conductance as introduced below.

This magnetization-dependent MBE can be further interpreted by magnon selection rules inside FMI and AFMI materials [Figs. 1(d) and 1(e)]. In general, spin-up (spin-down) lattices can only accommodate right- (left-) circularly polarized magnons. While only right-circularly polarized magnons are favored in FMI with ↑ magnetization [31,43,44], both left- and right-circular polarizations are permitted in AFMI owing to two spin-opposite lattices [45]. Moreover, linearly polarized magnons composed by equal partition of left- and right-circular components are also accommodated in AFMI [45]. This selection rule thus makes the MBE occur when magnons try to diffuse into a spin lattice, which does not support their polarization. For instance, when right-circular magnons excited in spin-up region are injected into the spin-down region, the selection rule would result in low magnon transmission across the interface. We also simulate the same model at $T_L = 0.5$ J and $T_R = 0.05$ J. Little difference is observed, demonstrating robustness of this mechanism against thermal fluctuation.

Next we turn to MJ with other kinds of AFMI spacers. Little MJE (MBR = 0) is observed in the type-A AFMI spacer whose spin vector lies in the y direction [Figs. 2(a) and 2(b)], which is naturally explained by the magnon selection rule as depicted in Figs. 2(c) and 2(d). In the P state, the right-circularly polarized magnons generated in FMI_1 can be decomposed into two linearly polarized components in x and y directions. Only the x component can diffuse into AFMI whose spin vector lies in the y direction. The x-polarized component can be further deemed as the sum of two circularly polarized magnons. Nevertheless, only the right-circular magnons match the FMI_2 layer and can be injected eventually. A similar process occurs in the AP state, resulting in the same magnon transmission [Fig. 2(d)].

We also investigate the type-C spacer without next-neighboring interaction ($J_{NN} = 0$). Similar to type A, the type C spacer also makes the MJE clearly observed. However, the magnon potential in the FMI_2 region for the latter [Fig. 2(e)] is much lower than that in the type-A case [Fig. 1(b)], especially for the P state, showing stronger MBE at the interfaces for the type-C spacer.

After a next-neighboring interaction ($J_{NN} = 0.1$ J) in AFMI is taken into account, magnon transmission in the P state as characterized by the $\delta|M_z|$ in FMI_2 region significantly increases. For example, for the case of $J_{NN} = 0.1$ J, $\delta|M_z(200)| = 8 \times 10^{-5}$ is larger than $\delta|M_z(200)| = 1 \times 10^{-5}$ for $J_{NN} = 0$. This phenomenon is also rooted in the polarization-dependent magnon blocking in atomic scale as depicted in Figs. 2(g)–2(j). In type-C AFMI with $J_{NN} = 0$, injected right-handed magnons have to flow through both spin-up (⊙) and spin-down sites (⊗). As mentioned before, the right-handed magnons can only be accommodated in the spin-down sublattice, so the spin-down sites act as magnon blocking sites for the injected right-handed magnons. Fortunately, after introducing the next-neighboring interaction, magnons can bypass those blocking sites, thus enhancing magnon transmission.

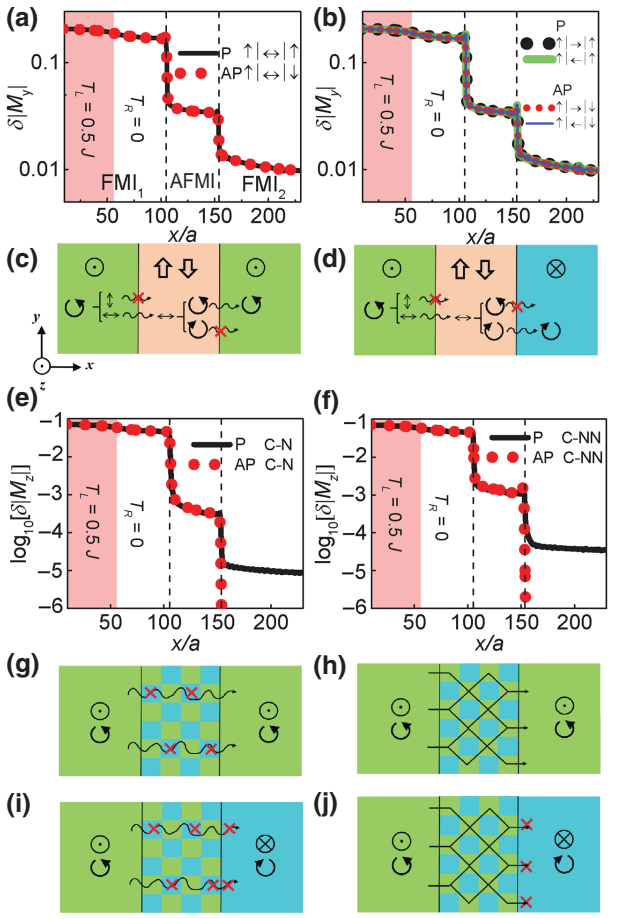

FIG. 2. Magnon transmission of different AFMI-based MJs at $J_c = 0.3$ J, $T_L = 0.5$ J, and $T_R = 0$. Simulated total $\delta|M_x|$ (a) and its channel resolution (b) of 9° rotated of AFMI-spacer-based MJ. (c),(d) Process of polarization transition and magnon blocking of P and AP state, respectively. Magnon transmission in MJ without next-neighbor interaction in type-C AFMI spacer are given in (e), (g), and (i) and the similar one with next-neighbor interaction are given in (f), (h), and (j).

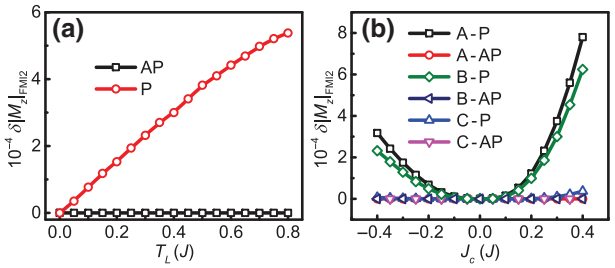

FIG. 3. Transmitted magnon ($\delta|M_z|_{\mathrm{FMI2}}$) as a function of temperature in the magnon source region (T_L) and interfacial coupling between AFMI and FMI layer (J_c) at $T_R = 0$. Average magnon potential in the bulk region of FMI_2 is used to evaluate the transmitted magnon. The type-A AFMI spacer and $J_c = 0.3$ J is considered in (a) and three different types of AFMI spacers are investigated in (b) at $T_L = 0.5$ J.

In short, the type-A AFMI spacer has the best performance in producing large MJE. Actually, the type-B AFMI spacer also shows good magnon transmission, whose mechanism is the same as type A. Similar results are shown in Fig. 3 later. For future experiments of optimizations of MJs' structures, promising materials with the type-A and type-B AFMI spacer to implement our model are Cr_2O_3[100] [46] or NiO[$1\bar{1}0$] [47] and type-C can be Cr_2O_3[$1\bar{1}0$] or NiO[001] and ferromagnetic insulator electrode could be YIG, $NiFe_2O_4$. Though behaving as fluid, magnons also show some wave features in our model. Magnons are excited and diffuse from the hot to the cold end according to the Boltzmann or Navier-Stokes equation as explored by numbers of previous work [24,48]. These studies demonstrate the particle nature of magnons very well. However, when the case comes to magnon injection and transmission across an interface between two spin-ordered materials, intrinsic magnon modes bearing polarization information have to be considered. Those intrinsic modes determine precessional manners of how spin lattices vibrate. Thus magnons also show wave nature when analyzing their transmission across different mediums.

The magnon transmission in a MJ is also modulated by the temperature step and the interfacial coupling as illustrated in Fig. 3. $\delta|M_z|_{\mathrm{FMI2}}$ is used to evaluate the transmitted magnon from FMI_1 to FMI_2. When T_L is tuned larger, $\delta|M_z|_{\mathrm{FMI2}}$ increases as expected because of higher magnon potential in the hot region and a larger driving force for magnon current. Similar results in the system of single ferromagnetic layer have been observed in experiments and simulations [11,40,41,49]. The interfacial coupling between FMI and AFMI also plays a role in magnon transmission. $\delta|M_z|_{\mathrm{FMI2}}$ increases as is J_c enhanced, demonstrating the increase in the density of transmitted magnons. It should be pointed out that we only consider $|J_c| < 0.4$. Higher $|J_c|$ than 0.4 causes spin-flop transitions and noncollinear spin structures due to frustration in the interface, which is beyond the scope of this paper. We also give the results of different types of AFMI spacers in Fig. 3(b). It shows that type A and type B have higher $\delta|M_z|_{\mathrm{FMI2}}$ than type C at the same J_c and T_L demonstrating that type A and type B have better magnon transmission, consistent with the proposed mechanism of the magnon selection rules. In addition to the various types of AFMI we discuss, another type of AFMI spacer (the interlayer antiferromagnetic order with in-plane ferromagnetic order) is also significant and MJ with this spacer have been theoretically investigated by previous works (as shown in Figs. S8–10 within the Supplemental Material [31]). This model also shows the MJE induced by the magnon selection rules. It is noteworthy that while Ref. [31] deals with coherent magnons, we treat thermal magnons without phase coherence. The magnon selection rules seemly hold for both cases.

By use of the Holstein-Primakoff transform [50] and the linear spin-wave approximation [51], the calculated magnon energy gap of types A, B, and C are around 0.3, 0.4, and 0.5 J, respectively. Compared to the energy gap of the FM layer (0.02 J), their gaps are much larger. Some previous works show that the injected magnons with frequency below the AFM gap frequencies are in evanescent modes with a spatial decay, and normal modes excited above the frequency gap have a longer propagation length [31,52,53]. As the frequency increases, the decay length of evanescent modes increases, leading to the magnons of evanescent modes with high frequency having a large possibility to propagate through AFM layer. On the other hand, the thickness of the AFM also influences the transmission of evanescent-mode magnons. If the decay length is smaller than the thickness of AFM layer, the transmission coefficient of evanescent-mode magnons cannot be neglected. Thus, for the thick enough AFM spacer, magnons with frequency below but near the gap of the AFM spacer or with higher frequency than the gap can be transmitted from FMI_1 to FMI_2. According to the pioneering reports [40], the frequency distribution of thermal magnons shows that as frequency increases the proportion of amplitude contribution decreases, so the frequencies which are around the gap frequency of AFM spacer contribute dominantly to the transmitted signal.

Based on our MJ model, we further simulate MJE under the following condition of strong interlayer coupling ($J_c = 1$ J), thin thickness of AFMI layer ($L_{\mathrm{AFMI}} = 1$–6) and temperature gradient (7.8×10^{-4} J/a) across the whole MJ as experimentally demonstrated in Ref. [14]. We find experimental results of MJE (or MVE) can be semiquantitatively reproduced (not shown here) [14] due to the MBE induced by the magnon selection rules.

Besides of the longitudinal MJE, here, we propose and investigate another in-plane MJE based on the above picture. The schematics of a nonlocal transport device is presented in Fig. 4(a). In practice, magnon injection into the top layer can be realized by spin Hall

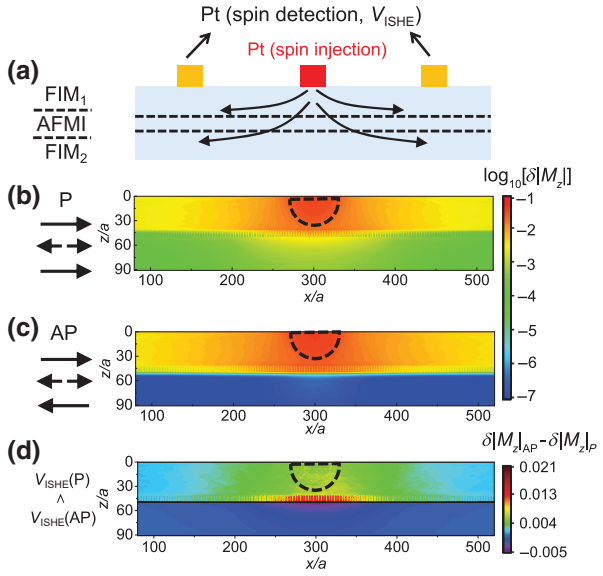

FIG. 4. In-plane magnon junction effect in nonlocal spin-transport device. (a) Schematics of the nonlocal spin-transport geometry. Two heavy metallic leads are used for spin injection and detection on the FMI_1-AFMI-FMI_2 MJ structure. Spatial dependence of simulated magnon potential of the P and AP state are given in (b),(c). Localized spin injection is induced by temperature step, where temperature in arc and out of arc regions are 0.5 and 0 J, respectively. (d) Difference of magnon potential between AP and P state. Due to MBE in AP state, magnon potential in the top FMI layer of the P state is larger. Thus, the detected spin signal by inverse spin Hall effect of P states V_{ISHE} (P) should be smaller than V_{ISHE} (AP).

[9–12,15,48] or spin Seebeck effect [10,13,14]. The other metallic stripe works as a spin detector based on inverse spin Hall effect [10,11,13,14,16,48,54]. In simulation, we set a temperature step around the injector and spin-sink boundary is considered in the right and left end. The spatial distribution of magnon potential at the P or AP state is shown in Figs. 4(b) and 4(c). Due to the MBE, $\delta|M_z|$ in the bottom FMI layer is different for the two states. The detected signal actually depends on the magnon current in the top layer. In order to clearly show the influence of the P and AP states on magnon transport, we calculate the difference in magnon potential between the two states $\delta|M_z|_{AP}(x,z) - \delta|M_z|_P(x,z)$ and find $\delta|M_z|_{AP}(x,z) - \delta|M_z|_P(x,z) > 0$ with $z < 40$, showing that in any position of the top FMI layer magnon potential in the AP state is always higher than in the P state. It demonstrates that the majority of magnon current is constrained within the top FMI layer for the AP state, so the detected spin signal in this case is larger.

IV. CONCLUSIONS

In summary, we investigate the magnon transmission in AFMI-based MJ by atomic spin dynamics simulations. We reproduce the MJE and reveal that it stemmed from spin-dependent MBE. Furthermore, the magnon transmission in a MJ can be remarkably changed by the AFMI spacers with various configurations. Based on these properties and mechanisms, we propose an in-plane MJ in which the spin signal is higher for the AP state than the P state. Our works can provide significant and meaningful information for both the fundamental physics and the appealing application of MJ devices.

ACKNOWLEDGMENTS

This work is supported by the National Key Research and Development Program of China (MOST, Grants No. 2017YFA0206200 and No. 2016YFA0300802), the National Natural Science Foundation of China (NSFC, Grants No. 51831012, No. 51620105004, and No. 11974398), Beijing Natural Science Foundation (Grant No. Z201100004220006) and partially supported by the Strategic Priority Research Program (B) (Grant No. XDB33000000), the International Partnership Program (Grant No. 112111KYSB20170090), and the Key Research Program of Frontier Sciences (Grant No. QYZDJSSWSLH016) of the Chinese Academy of Sciences (CAS). C.H. Wan appreciates financial support from Youth Innovation Promotion Association, CAS (Grant No. 2020008).

[1] S. Neusser and D. Grundler, Magnonics: Spin waves on the nanoscale, Adv. Mater. **21**, 2927 (2009).
[2] V. Kruglyak, S. Demokritov, and D. Grundler, Magnonics, J. Phys. D **43**, 264001 (2010).
[3] A. V. Chumak, V. I. Vasyuchka, A. A. Serga, and B. Hillebrands, Magnon spintronics, Nat. Phys. **11**, 453 (2015).
[4] Y. Kajiwara, K. Harii, S. Takahashi, J.-I. Ohe, K. Uchida, M. Mizuguchi, H. Umezawa, H. Kawai, K. Ando, K. Takanashi, S. Maekawa, and E. Saitoh, Transmission of electrical signals by spin-wave interconversion in a magnetic insulator, Nature **464**, 262 (2010).
[5] D. Wesenberg, T. Liu, D. Balzar, M. Wu, and B. L. Zink, Long-distance spin transport in a disordered magnetic insulator, Nat. Phys. **13**, 987 (2017).
[6] C. Liu, J. Chen, T. Liu, F. Heimbach, H. Yu, Y. Xiao, J. Hu, M. Liu, H. Chang, T. Stueckler, S. Tu, Y. Zhang, Y. Zhang, P. Gao, Z. Liao, D. Yu, K. Xia, N. Lei, W. Zhao, and M. Wu, Long-distance propagation of short-wavelength spin waves, Nat. Commun. **9**, 738 (2018).
[7] H. Yu, O. D. Kelly, V. Cros, R. Bernard, P. Bortolotti, A. Anane, F. Brandl, R. Huber, I. Stasinopoulos, and D. Grundler, Magnetic thin-film insulator with ultra-low spin wave damping for coherent nanomagnonics, Sci. Rep. **4**, 6848 (2014).
[8] G. Talmelli, F. Ciubotaru, K. Garello, X. Sun, M. Heyns, I. P. Radu, C. Adelmann, and T. Devolder, Spin-Wave Emission by Spin-Orbit-Torque Antennas, Phys. Rev. Appl. **10**, 044060 (2018).

[9] S. S.-L. Zhang and S. Zhang, Magnon Mediated Electric Current Drag Across a Ferromagnetic Insulator Layer, Phys. Rev. Lett. **109**, 096603 (2012).

[10] L. Cornelissen, J. Liu, R. Duine, J. B. Youssef, and B. Van Wees, Long-distance transport of magnon spin information in a magnetic insulator at room temperature, Nat. Phys. **11**, 1022 (2015).

[11] H. Wu, C. H. Wan, X. Zhang, Z. H. Yuan, Q. T. Zhang, J. Y. Qin, H. X. Wei, X. F. Han, and S. Zhang, Observation of magnon-mediated electric current drag at room temperature, Phys. Rev. B **93**, 060403 (2016).

[12] J. Li, Y. Xu, M. Aldosary, C. Tang, Z. Lin, S. Zhang, R. Lake, and J. Shi, Observation of magnon-mediated current drag in Pt/yttrium iron garnet/Pt (Ta) trilayers, Nat. Commun. **7**, 10858 (2016).

[13] H. Wu, L. Huang, C. Fang, B. S. Yang, C. H. Wan, G. Q. Yu, J. F. Feng, H. X. Wei, and X. F. Han, Magnon Valve Effect between Two Magnetic Insulators, Phys. Rev. Lett. **120**, 097205 (2018).

[14] C. Y. Guo, C. H. Wan, X. Wang, C. Fang, P. Tang, W. Kong, M. K. Zhao, L. Jiang, B. S. Tao, G. Q. Yu, and X. F. Han, Magnon valves based on YIG/NiO/YIG all-insulating magnon junctions, Phys. Rev. B **98**, 134426 (2018).

[15] C. Y. Guo, C. H. Wan, W. Q. He, M. K. Zhao, Z. R. Yan, Y. W. Xing, X. Wang, P. Tang, Y. Z. Liu, S. Zhang, Y. W. Liu, and X. F. Han, A nonlocal spin Hall magnetoresistance in a platinum layer deposited on a magnon junction, Nat. Electron. **3**, 304 (2020).

[16] K. S. Das, J. Liu, B. J. van Wees, and I. J. Vera-Marun, Efficient injection and detection of out-of-plane spins via the anomalous spin Hall effect in permalloy nanowires, Nano Lett. **18**, 5633 (2018).

[17] C. Liu, S. Wu, J. Zhang, J. Chen, J. Ding, J. Ma, Y. Zhang, Y. Sun, S. Tu, H. Wang, P. Liu, C. Li, Y. Jiang, P. Gao, D. Yu, J. Xiao, R. Duine, M. Wu, C.-W. Nan, J. Zhang, and H. Yu, Current-controlled propagation of spin waves in antiparallel, coupled domains, Nat. Nanotechnol. **14**, 691 (2019).

[18] C. Y. Guo, C. H. Wan, M. K. Zhao, H. Wu, C. Fang, Z. R. Yan, J. F. Feng, H. F. Liu, and X. F. Han, Spin-orbit torque switching in perpendicular $Y_3Fe_5O_{12}$/Pt bilayer, Appl. Phys. Lett. **114**, 192409 (2019).

[19] L. Cornelissen, J. Liu, B. Van Wees, and R. Duine, Spin-Current-Controlled Modulation of the Magnon Spin Conductance in a Three-Terminal Magnon Transistor, Phys. Rev. Lett. **120**, 097702 (2018).

[20] R. Doornenbal, A. Roldán-Molina, A. Nunez, and R. Duine, Spin-Wave Amplification and Lasing Driven by Inhomogeneous Spin-Transfer Torques, Phys. Rev. Lett. **122**, 037203 (2019).

[21] A. Navabi, Y. Liu, P. Upadhyaya, K. Murata, F. Ebrahimi, G. Yu, B. Ma, Y. Rao, M. Yazdani, M. Montazeri, L. Pan, I. N. Krivorotov, I. Barsukov, Q. Yang, P. Khalili Amiri, Y. Tserkovnyak, and K. L. Wang, Control of Spin-Wave Damping in YIG Using Spin Currents from Topological Insulators, Phys. Rev. Appl. **11**, 034046 (2019).

[22] A. Roldán-Molina, A. S. Nunez, and R. Duine, Magnonic Black Holes, Phys. Rev. Lett. **118**, 061301 (2017).

[23] R. Verba, M. Carpentieri, G. Finocchio, V. Tiberkevich, and A. Slavin, Excitation of propagating spin waves in ferromagnetic nanowires by microwave voltage-controlled magnetic anisotropy, Sci. Rep. **6**, 25018 (2016).

[24] Y. Cheng, K. Chen, and S. Zhang, Giant magneto-spin-Seebeck effect and magnon transfer torques in insulating spin valves, Appl. Phys. Lett. **112**, 052405 (2018).

[25] R. Cheng, D. Xiao, and J.-G. Zhu, Antiferromagnet-based magnonic spin-transfer torque, Phys. Rev. B **98**, 020408 (2018).

[26] Y. Chen, E. Cogulu, D. Roy, J. Ding, J. B. Mohammadi, P. G. Kotula, N. A. Missert, M. Wu, and A. D. Kent, Spin transport in an insulating ferrimagnetic-antiferromagnetic-ferrimagnetic trilayer as a function of temperature, AIP Adv. **9**, 105319 (2019).

[27] S. J. Hämäläinen, M. Madami, H. Qin, G. Gubbiotti, and S. van Dijken, Control of spin-wave transmission by a programmable domain wall, Nat. Commun. **9**, 4853 (2018).

[28] A. V. Chumak, A. A. Serga, and B. Hillebrands, Magnon transistor for all-magnon data processing, Nat. Commun. **5**, 4700 (2014).

[29] J. Lan, W. Yu, R. Wu, and J. Xiao, Spin-Wave Diode, Phys. Rev. X **5**, 041049 (2015).

[30] P. Tang and X. F. Han, Magnon resonant tunneling effect in double-barrier insulating magnon junctions and magnon field effect transistor, Phys. Rev. B **99**, 054401 (2019).

[31] J. Cramer, F. Fuhrmann, U. Ritzmann, V. Gall, T. Niizeki, R. Ramos, Z. Qiu, D. Hou, T. Kikkawa, J. Sinova, U. Nowak, E. Saitoh, and M. Kläui, Magnon detection using a ferroic collinear multilayer spin valve, Nat. Commun. **9**, 1089 (2018).

[32] M. Julliere, Tunneling between ferromagnetic films, Phys. Lett. A **54**, 225 (1975).

[33] M. N. Baibich, J. M. Broto, A. Fert, F. N. Van Dau, F. Petroff, P. Etienne, G. Creuzet, A. Friederich, and J. Chazelas, Giant Magnetoresistance of (001)Fe/(001)Cr Magnetic Superlattices, Phys. Rev. Lett. **61**, 2472 (1988).

[34] G. Binasch, P. Grünberg, F. Saurenbach, and W. Zinn, Enhanced magnetoresistance in layered magnetic structures with antiferromagnetic interlayer exchange, Phys. Rev. B **39**, 4828 (1989).

[35] S. Zhang and P. M. Levy, Conductivity perpendicular to the plane of multilayered structures, J. Appl. Phys. **69**, 4786 (1991).

[36] T. Miyazaki and N. Tezuka, Giant magnetic tunneling effect in $Fe/Al_2O_3/Fe$ junction, J. Magn. Magn. Mater. **139**, L231 (1995).

[37] J. Mathon and A. Umerski, Theory of tunneling magnetoresistance of an epitaxial Fe/MgO/Fe (001) junction, Phys. Rev. B **63**, 220403 (2001).

[38] W. Butler, X.-G. Zhang, T. Schulthess, and J. MacLaren, Spin-dependent tunneling conductance of Fe/MgO/Fe sandwiches, Phys. Rev. B **63**, 054416 (2001).

[39] K. Wright, A trio of magnon transistors, Physics **11**, 23 (2018).

[40] U. Ritzmann, D. Hinzke, and U. Nowak, Propagation of thermally induced magnonic spin currents, Phys. Rev. B **89**, 024409 (2014).

[41] U. Ritzmann, D. Hinzke, and U. Nowak, Thermally induced magnon accumulation in two-sublattice magnets, Phys. Rev. B **95**, 054411 (2017).
[42] U. Nowak, in *Handbook of Magnetism and Advanced Magnetic Materials*, edited by H. Kronmüller, S. Parkin, J. E. Miltat, and M. R. Scheinfein (Wiley, New York, 2007).
[43] Z. Zhou, X. Wang, Y. Nie, Q. Xia, Z. Zeng, and G. Guo, Left-handed polarized spin waves in ferromagnets induced by spin-transfer torque, Phys. Rev. B **99**, 014420 (2019).
[44] J. Lan, W. Yu, and J. Xiao, Manipulating spin wave polarization in synthetic antiferromagnet, arXiv:1810.12149 (2018).
[45] J. Lan, W. Yu, and J. Xiao, Antiferromagnetic domain wall as spin wave polarizer and retarder, Nat. Commun. **8**, 178 (2017).
[46] J. Dho, M. Blamire, and E. Chi, Correlation of the exchange interaction in $Ni_{81}Fe_{19}/Cr_2O_3$ bilayers with the antiferromagnetic spin configuration, Phys. Rev. B **72**, 224421 (2005).
[47] W. Roth, Neutron and optical studies of domains in NiO, J. Appl. Phys. **31**, 2000 (1960).
[48] C. Ulloa, A. Tomadin, J. Shan, M. Polini, B. Van Wees, and R. Duine, Nonlocal Spin Transport as a Probe of Viscous Magnon Fluids, Phys. Rev. Lett. **123**, 117203 (2019).
[49] U. Ritzmann, D. Hinzke, A. Kehlberger, E.-J. Guo, M. Kläui, and U. Nowak, Magnetic field control of the spin Seebeck effect, Phys. Rev. B **92**, 174411 (2015).
[50] T. Holstein and H. Primakoff, Field dependence of the intrinsic domain magnetization of a ferromagnet, Phys. Rev. **58**, 1098 (1940).
[51] P. W. Anderson, An approximate quantum theory of the antiferromagnetic ground state, Phys. Rev. **86**, 694 (1952).
[52] R. Khymyn, I. Lisenkov, V. S. Tiberkevich, A. N. Slavin, and B. A. Ivanov, Transformation of spin current by antiferromagnetic insulators, Phys. Rev. B **93**, 224421 (2016).
[53] J. Cramer, U. Ritzmann, B.-W. Dong, S. Jaiswal, Z. Qiu, E. Saitoh, U. Nowak, and M. Kläui, Spin transport across antiferromagnets induced by the spin Seebeck effect, J. Phys. D: Appl. Phys **51**, 144004 (2018).
[54] R. Lebrun, A. Ross, S. Bender, A. Qaiumzadeh, L. Baldrati, J. Cramer, A. Brataas, R. Duine, and M. Kläui, Tunable long-distance spin transport in a crystalline antiferromagnetic iron oxide, Nature **561**, 222 (2018).